ARMY RESEARCH LABORATORY

Application of Computational Fluid Dynamics to a Monoplane Fixed-Wing Missile With Elliptic Cross Sections

by Karen Heavey and Jubaraj Sahu

ARL-TR-3549 **July 2005**

NOTICES

Disclaimers

The findings in this report are not to be construed as an official Department of the Army position unless so designated by other authorized documents.

Citation of manufacturer's or trade names does not constitute an official endorsement or approval of the use thereof.

Destroy this report when it is no longer needed. Do not return it to the originator.

Army Research Laboratory
Aberdeen Proving Ground, MD 21005-5066

ARL-TR-3549 **July 2005**

Application of Computational Fluid Dynamics to a Monoplane Fixed-Wing Missile With Elliptic Cross Sections

Karen Heavey and Jubaraj Sahu
Weapons and Materials Research Directorate, ARL

REPORT DOCUMENTATION PAGE

Form Approved
OMB No. 0704-0188

1. REPORT DATE *(DD-MM-YYYY)*	2. REPORT TYPE	3. DATES COVERED (From - To)
July 2005	Final	January 2003–December 2004

4. TITLE AND SUBTITLE
Application of Computational Fluid Dynamics to a Monoplane Fixed-Wing Missile With Elliptic Cross Sections

5a. CONTRACT NUMBER

5b. GRANT NUMBER

5c. PROGRAM ELEMENT NUMBER

6. AUTHOR(S)
Karen Heavey and Jubaraj Sahu

5d. PROJECT NUMBER
622617.H8000

5e. TASK NUMBER

5f. WORK UNIT NUMBER

7. PERFORMING ORGANIZATION NAME(S) AND ADDRESS(ES)
U.S. Army Research Laboratory
ATTN: AMSRD-ARL-WM-BC
Aberdeen Proving Ground, MD 21005-5066

8. PERFORMING ORGANIZATION REPORT NUMBER
ARL-TR-3549

9. SPONSORING/MONITORING AGENCY NAME(S) AND ADDRESS(ES)

10. SPONSOR/MONITOR'S ACRONYM(S)

11. SPONSOR/MONITOR'S REPORT NUMBER(S)

12. DISTRIBUTION/AVAILABILITY STATEMENT
Approved for public release; distribution is unlimited.

13. SUPPLEMENTARY NOTES

14. ABSTRACT
This report describes a computational study undertaken to investigate the performance of the CFD++ flow solver for prediction of nonlinear aerodynamics of a complex finned missile using structured hexahedral and unstructured tetrahedral grids. A monoplane fixed-wing missile with elliptic cross sections provided a geometrically complex model. Numerical solutions were obtained for this configuration at supersonic speed for various roll orientations, angles of attack, and jaw angles. Steady-state solutions were obtained using a three-dimensional Reynolds-Averaged Navier-Stokes solver with a two-equation turbulence model. Numerical results show the qualitative features of the flow fields at various cross-sectional and streamwise positions along the computational model of the missile. Aerodynamic coefficients were extracted from the computed solutions and found to match well with the available experimental data for these configurations. These numerical results show the effectiveness of using computational fluid dynamics techniques to produce an accurate prediction of the aerodynamics of geometrically complete configurations.

15. SUBJECT TERMS
monoplane fixed-wing, elliptic, computational fluid dynamics, experimental data

16. SECURITY CLASSIFICATION OF:			17. LIMITATION OF ABSTRACT	18. NUMBER OF PAGES	19a. NAME OF RESPONSIBLE PERSON
a. REPORT	b. ABSTRACT	c. THIS PAGE			Karen Heavey
UNCLASSIFIED	UNCLASSIFIED	UNCLASSIFIED	UL	38	19b. TELEPHONE NUMBER (*Include area code*) 410-278-2916

Standard Form 298 (Rev. 8/98)
Prescribed by ANSI Std. Z39.18

Contents

List of Figures

List of Tables

Acknowledgments

This work was accomplished as part of the Technical Cooperation Program between the United States, Canada, the United Kingdom, and Australia on Weapons Technical Panel TP-2 Key Technology Area 2–19. The authors would like to thank Jerry Allen from the National Aeronautics and Space Administration (NASA) Langley Research Center and Victor Burnley from the U.S. Air Force Research Laboratory for providing the structured and unstructured grid for the NASA missile case, respectively. The authors also wish to thank Sukumar Chakravarthy from Metacomp Technologies for his expert technical advice. The computational support of the U.S. Army Research Laboratory Major Shared Resource Center is greatly appreciated.

1. Introduction

The prediction of aerodynamic coefficients for projectile configurations is essential in assessing the performance of new designs. Accurate determination of aerodynamics is critical to the low-cost development of new advanced guided projectiles, rockets, missiles, and smart munitions. Fins, canards, and jets can be used to provide control for maneuvering projectiles and missiles. The flow fields associated with these control mechanisms for the modern weapons are complex, involving three-dimensional (3-D) shock-boundary layer interactions and highly viscous dominated separated flow regions (*1–5*). Computational fluid dynamics (CFD) has emerged as a critical technology for the aerodynamic design and assessment of weapons. Improved computer technology and state-of-the-art numerical procedures enable solutions to complex, 3-D problems associated with projectile and missile aerodynamics. In general, these techniques produce accurate and reliable numerical results for simple projectile and missile configurations at small angles of attack.

Modern weapons and the associated flow fields have increased in complexity as a result of changing military requirements. An increasing number of new weapon configurations are beyond the scope of traditional engineering prediction methods. Modern projectiles and missiles are expected to experience moderate to large angles of attack during flight. The flow field surrounding a slender missile at incidence features flow separations both from smooth bodies and sharp-edged lifting and control surfaces. Body and wing vortices (*6*, *7*) can dominate the flow field and interact with one another resulting in a very complex flow field even for simple geometries. Earlier work (*8*) on modeling of high angle of attack flow fields for finned missile configurations was initiated as part of the Technical Cooperation Program (TTCP) effort with participants from Canada, the United Kingdom, Australia, and the United States. This study addressed the application of Navier-Stokes methods to the prediction of flows around finned missile configurations and assessed the capabilities of Navier-Stokes solvers for the prediction of missile flow field at moderate to high angles of attack. It promoted technical interchange between aerodynamics specialists in the areas of grid generation, algorithms, turbulence modeling, and flow field visualization. The results of this study were reported in a special session of the American Institute of Aeronautics and Astronautics (AIAA) Applied Aerodynamics Conference in August 2000 (*8–10*). The study has shown that all Navier-Stokes methods employed were capable of providing accurate predictions of the overall normal force and pitching moment characteristics, even at very high angles of attack. However, some significant discrepancies in the prediction of the axial force were evident. In general, the agreement between computed and measured flow fields was good. Higher order turbulence models such as the k-ε models did not provide better accuracy compared to simpler algebraic

and one-equation models. The next phase of the research was to extend the scope of that study and to undertake a follow-on study to apply CFD technology to the prediction of aerodynamic flow fields for nonaxisymmetric missile configurations.

Maneuvering nonaxisymmetric missile configurations can be used for increased lethality and are being explored for future weapon systems in various scenarios. Additionally, nonaxisymmetric projectiles have been shown to generate large amounts of lift compared to conventional projectiles with circular cross sections (*11*). The aerodynamics of such configurations at high speeds are quite complex due to strong cross-flow influences and flow separation. Of particular interest was the accurate determination of supersonic and hypersonic flow over elliptic projectiles at moderate angles of attack. The flow field for such projectiles with nonaxisymmetric cross sections is complex, especially in the presence of jets used to maneuver these projectiles. This work was also initiated as part of another TTCP effort with international participants, and was aimed at assessing the capabilities of the both Euler and Navier-Stokes solvers currently available to research scientists for supersonic flow over elliptic projectiles for both jet-off and jet-on conditions (*12, 13*). This research effort also focused on the wind-tunnel testing as well as free-flight testing of these projectiles. Various aspects of computational techniques, such as grid generation, algorithms, turbulence modeling, and flow field visualization, were addressed by the group. The results of this study were reported in a special session of the AIAA Atmospheric Flight Mechanics Conference in August 2001. CFD approaches that included both Euler and Navier-Stokes schemes, structured and unstructured techniques, and a variety of turbulence models were used in the numerical simulations (*10–15*). In general, very good agreement of the computed aerodynamic coefficients with the experimental data was achieved at all angles of attack investigated for the jet-off uncontrolled conditions. Accurate prediction of the jet-on cases was found to be a little more challenging than the jet-off cases (*16*).

The TTCP efforts have continued recently with a focus on the application of CFD to missile aerodynamics which takes it to the next level of difficulty, that of multiple sets of fins and nonaxisymmetric configurations. Again, the objective was to compare the results obtained from Navier-Stokes computations against experimental data, evaluate the accuracy of the predictive technologies, and identify priorities for future development. The research focused on the application of advanced CFD techniques for accurate numerical prediction of supersonic flow over two nonaxisymmetric missile configurations, one with a square cross section and the other with an elliptic cross section; both have multiple sets of complex fins. Numerical computations for these complex configurations have been performed at supersonic speeds, for two roll orientations, for a range of angles of attack. Several cases were also computed with yaw angles. As with earlier efforts, these results were presented in conjunction with the other TTCP participants in a special session at the AIAA Applied Aerodynamics Conference in August 2004 (*17*).

The information presented in this U.S. Army Research Laboratory report focuses on the elliptic model only. Additional computational data that was not part of the TTCP effort are included in the report. A description of the computational techniques is presented, followed by a description of the applications of these techniques to the model at roll orientations of 0° and 45°. Computed results for these configurations are presented at Mach 2.5 at angles of attack ranging from 0° to 20°. The computed data are compared with experimental data provided by the National Aeronautics and Space Administration (NASA) Langley Research Center (*18*).

2. Solution Technique

2.1 CFD++ Flow Solver

A commercially available code, CFD++ (*19*, *20*), is used for the numerical simulations. The basic numerical framework in the code contains unified-grid, unified-physics, and unified-computing features. The user is referred to these references for details of the basic numerical framework. Here, only a brief synopsis of this framework and methodology is given.

The 3-D, Reynolds-averaged Navier-Stokes (*21*) equations are solved using the following finite volume method:

$$\frac{\partial}{\partial t}\int_V \mathrm{W}dV + \oint\left[\mathrm{F}-\mathrm{G}\right]\cdot dA = \int_V \mathrm{H}dV \ , \tag{1}$$

where W is the vector of conservative variables, F and G are the inviscid and viscous flux vectors, respectively, H is the vector of source terms, V is the cell volume, and A is the surface area of the cell face.

The numerical framework of CFD++ is based on the following general elements: (1) unsteady compressible and incompressible Navier-Stokes equations with turbulence modeling (unified-physics), (2) unification of Cartesian, structured curvilinear, and unstructured grids, including hybrids (unified-grid), (3) unification of treatment of various cell shapes including hexahedral, tetrahedral, and triangular prism cells (3-D), quadrilateral and triangular cells (2-D), and linear elements (1-D) (unified-grid), (4) treatment of multiblock patched aligned (nodally connected), patched nonaligned and overset grids (unified-grid), (5) total Variation Diminishing discretization based on a new multidimensional interpolation framework, (6) Riemann solvers to provide proper signal propagation physics, including versions for preconditioned forms of the governing equations, (7) consistent and accurate discretization of viscous terms using the same multidimensional polynomial framework, (8) pointwise turbulence models that do not require knowledge of distance to walls, (9) versatile boundary condition implementation includes a rich

variety of integrated boundary condition types for the various sets of equations, and (10) implementation on massively parallel computers based on the distributed-memory message-passing model using native message-passing libraries or MPI, PVM, etc. (unified-computing).

The code has brought together several ideas on convergence acceleration to yield a fast methodology for all flow regimes. The approach can be labeled as a "preconditioned-implicit-relaxation" scheme. It combines three basic ideas: implicit local time-stepping, relaxation, and preconditioning. Preconditioning the equations ideally equalizes the eigenvalues of the inviscid flux Jacobians and removes the stiffness arising from large discrepancies between the flow and sound velocities at low speeds. Use of an implicit scheme circumvents the stringent stability limits suffered by their explicit counterparts, and successive relaxation allows update of cells as information becomes available and thus aids convergence.

2.2 Numerical Technique

Second-order discretization was used for the flow variables and the turbulent viscosity equation. The turbulence closure was based on topology-parameter-free formulations. The realizable k-ε turbulence model (*22*) was used for the computation of turbulent flows for the missile configurations considered here. A pressure-temperature based inflow/outflow routine was utilized for the inflow, outflow, and farfield boundary conditions, while an adiabatic viscous wall condition was used on the missile surfaces – body, wings, and tailfins. A symmetry boundary condition was used along the *x*-axis in front of the missile for the hexahedral grid only. All calculations were performed at Mach number 2.5 using the experimental (wind tunnel) conditions: $Re = 5.56 \times 10^6/m$, $T_0 = 339$ K, $P_0 = 81.36$ kPa. This corresponds to a static temperature and pressure of 150.67 K and 4.76 kPa, respectively, for the CFD calculations.

Computations were performed using the various platforms available at the Major Shared Resource Center, to include SGI 3800 and IBM SP3 processors. The resources used, such as memory and CPU time, varied based on the mesh size. Most of the runs were done utilizing 16 or 24 processors. The next section describes the model geometries and the flow conditions for the elliptic cross-section NASA missile (*23, 24*).

3. Model Geometry and Numerical Grids

3.1 Projectile Model and Geometry

The geometric model for the elliptic missile is a sharp-nosed monoplane winged missile with tail fins. The overall body length is 0.7112 m with a 3:1 elliptical cross section, having maximum body width and height of 0.1760 m and 0.0587 m, respectively. There are four tail fins on the aft end of the missile, aligned with the base of the missile. This model, shown in figure 1, has been used extensively in wind tunnel tests at the NASA Langley Research Center (*18*).

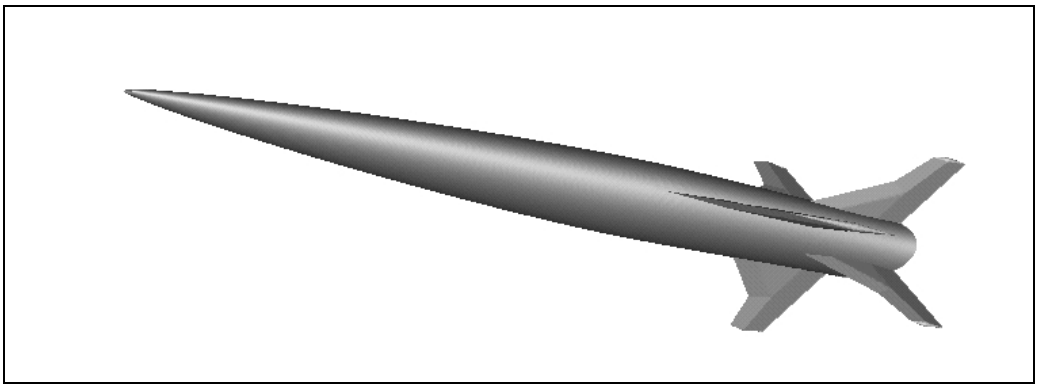

Figure 1. Computational model for the elliptic-section missile.

3.2 Computational Mesh

The focus of this study was to investigate the performance of the flow solver CFD++ using two different grid structures. The first grid was received as a structured mesh consisting of 3.8 million hexahedral cells. Figure 2 shows an expanded view of the grid in the aft region of the missile. This structured hexahedral mesh was provided by NASA Langley (*25*). The second grid is an unstructured mesh consisting of 2.9-million tetrahedral cells. A view of the surface mesh on the tail fins is shown in figure 3. This unstructured tetrahedral mesh was provided by the U.S. Air Force Research Laboratory (*26*).

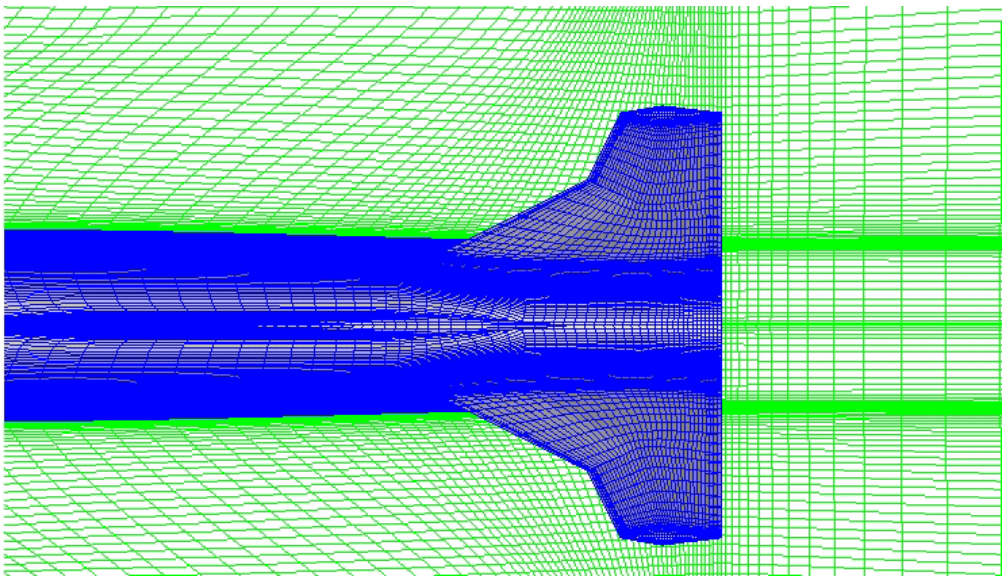

Figure 2. Expanded view of the hexahedral mesh in the aft region of the elliptic missile.

Since CFD++ requires a code-specific unstructured format for the input geometry, both computational meshes were converted prior to use with the flow solver. The conversion routine is included in the CFD++ graphical user interface (GUI) which was also used to set up the numerical input parameters.

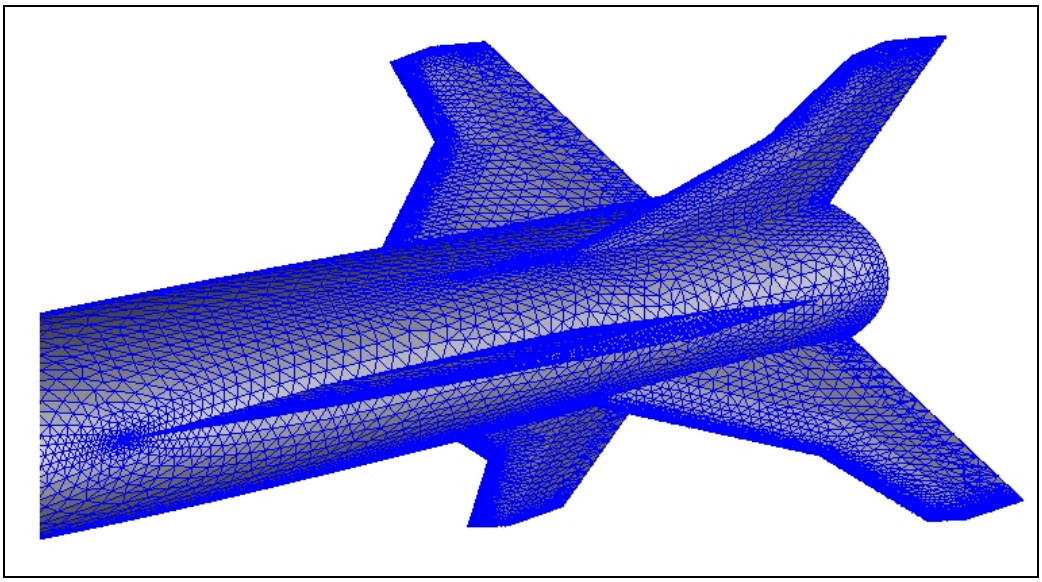

Figure 3. View of the tetrahedral mesh on the aft surface of the elliptic missile.

The original grids received had a roll orientation of 0°. A tool available within the CFD++ GUI was used to rotate each grid 45° on the *x*-axis. A series of computations was performed using each of these four grids.

4. Results and Discussion

Computations using viscous Navier-Stokes methods were performed to predict the flow field and aerodynamic coefficients for a monoplane fixed wing missile with elliptic cross section under wind tunnel test conditions, using the CFD++ flow solver at a supersonic Mach number of 2.5, at roll orientations of 0° and 45°, for angles of attack ranging from 0° to 20°. Several cases were also computed with yaw angles of 4.6° and 8.6°, at 0° and 20° angles of attack. Full 3-D calculations were performed and no symmetry was used. Computational results obtained for both the hexahedral mesh and tetrahedral mesh are presented both qualitatively and quantitatively. The results are then compared to experimental data.

Figures 4 and 5 are schematics of the axial and circumferential locations on the missile surface, normalized by the overall body length (L), at which the experimental data was collected (*18*). The numerical results are compared to available experimental data obtained at several of these positions.

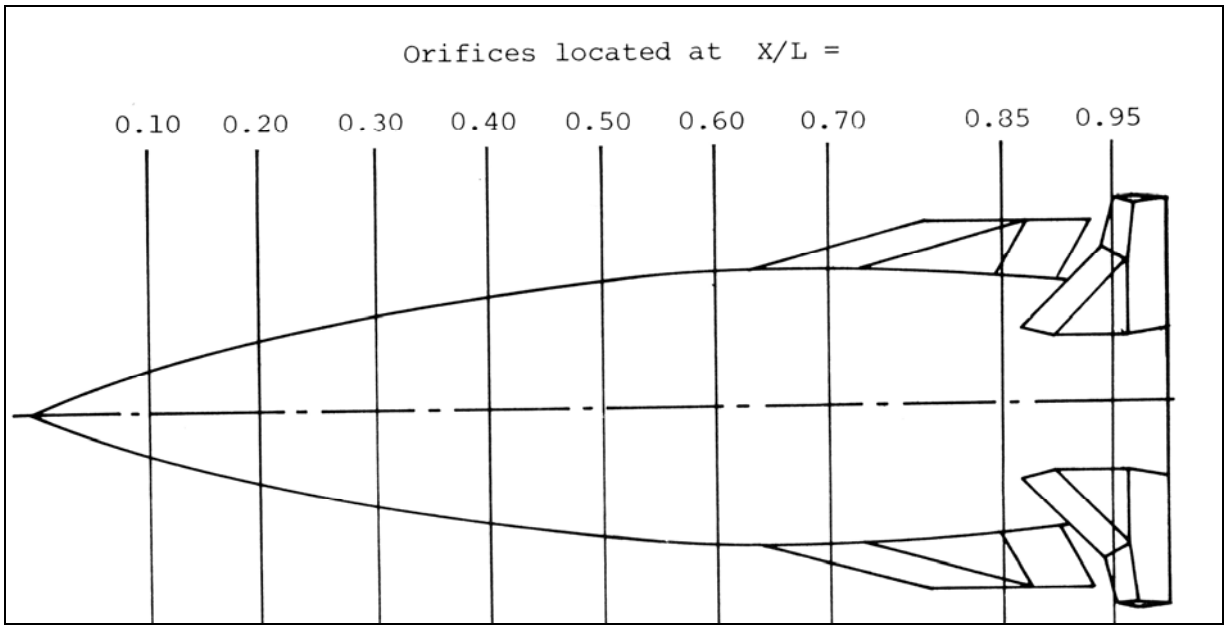

Figure 4. Axial locations for experimental data.

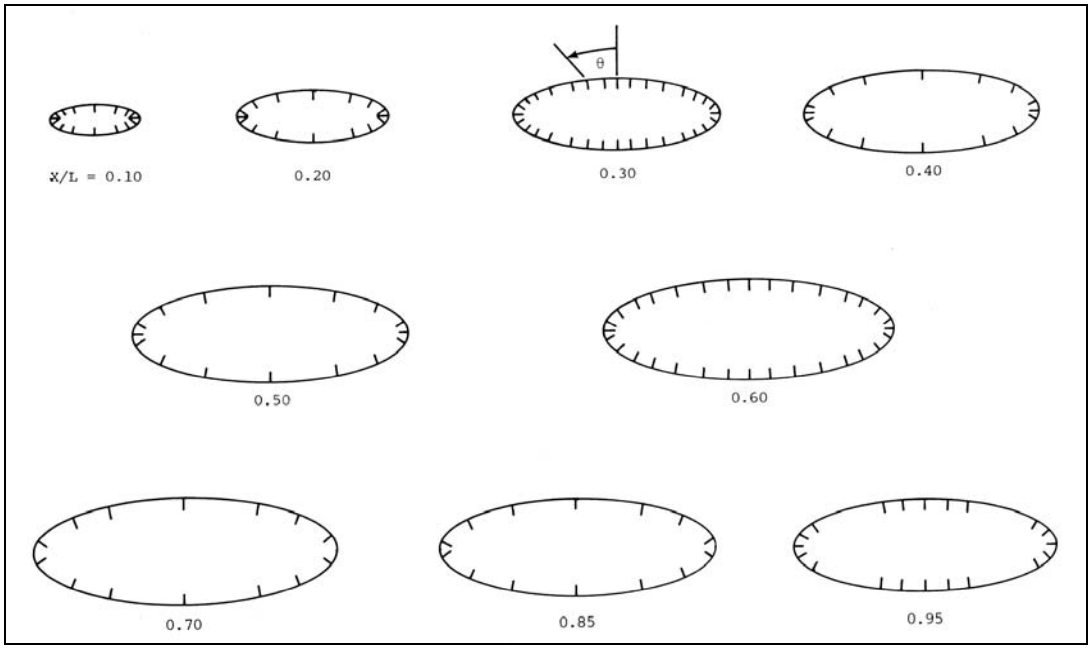

Figure 5. Circumferential locations of experimental data points.

4.1 Qualitative Results

Visualization of pressure on the missile surface appears to be the same for both the hexahedral and tetrahedral solutions, as seen in figure 6. However, Mach and Pressure contours show the flow field characteristics to be more defined in the solutions for the hexahedral mesh. The longitudinal Mach contours for the $y = 0$ pitch plane depicted in figure 7 show this to be

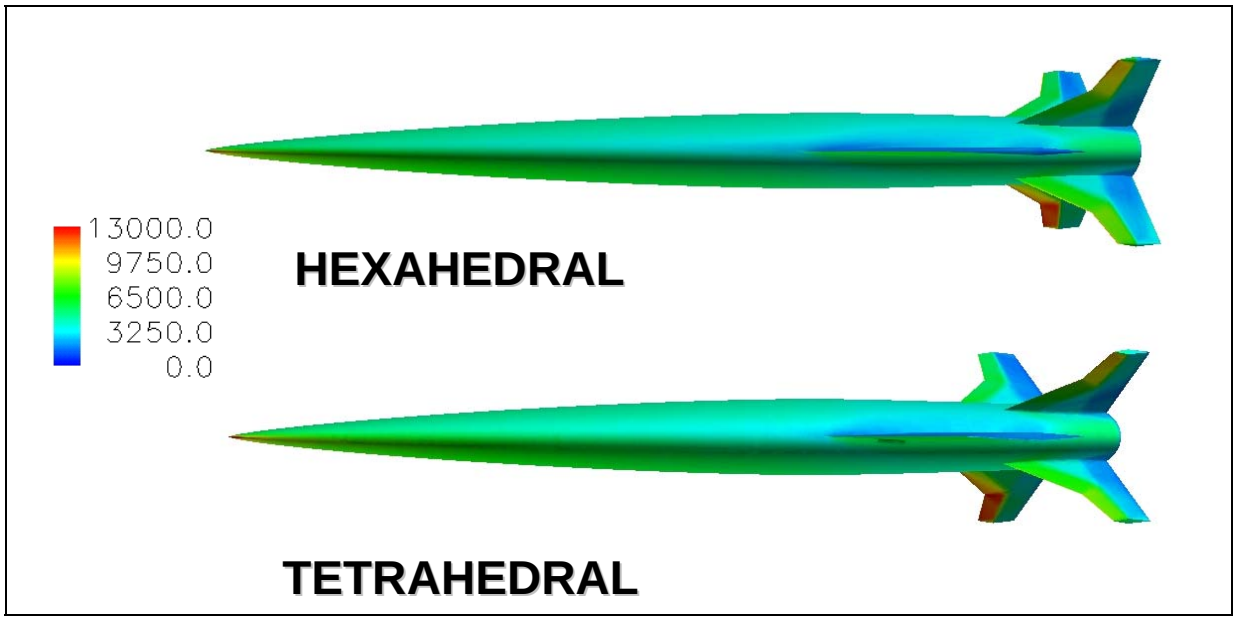

Figure 6. Surface pressure contours for $\alpha = 5°$, and $\phi = 0°$.

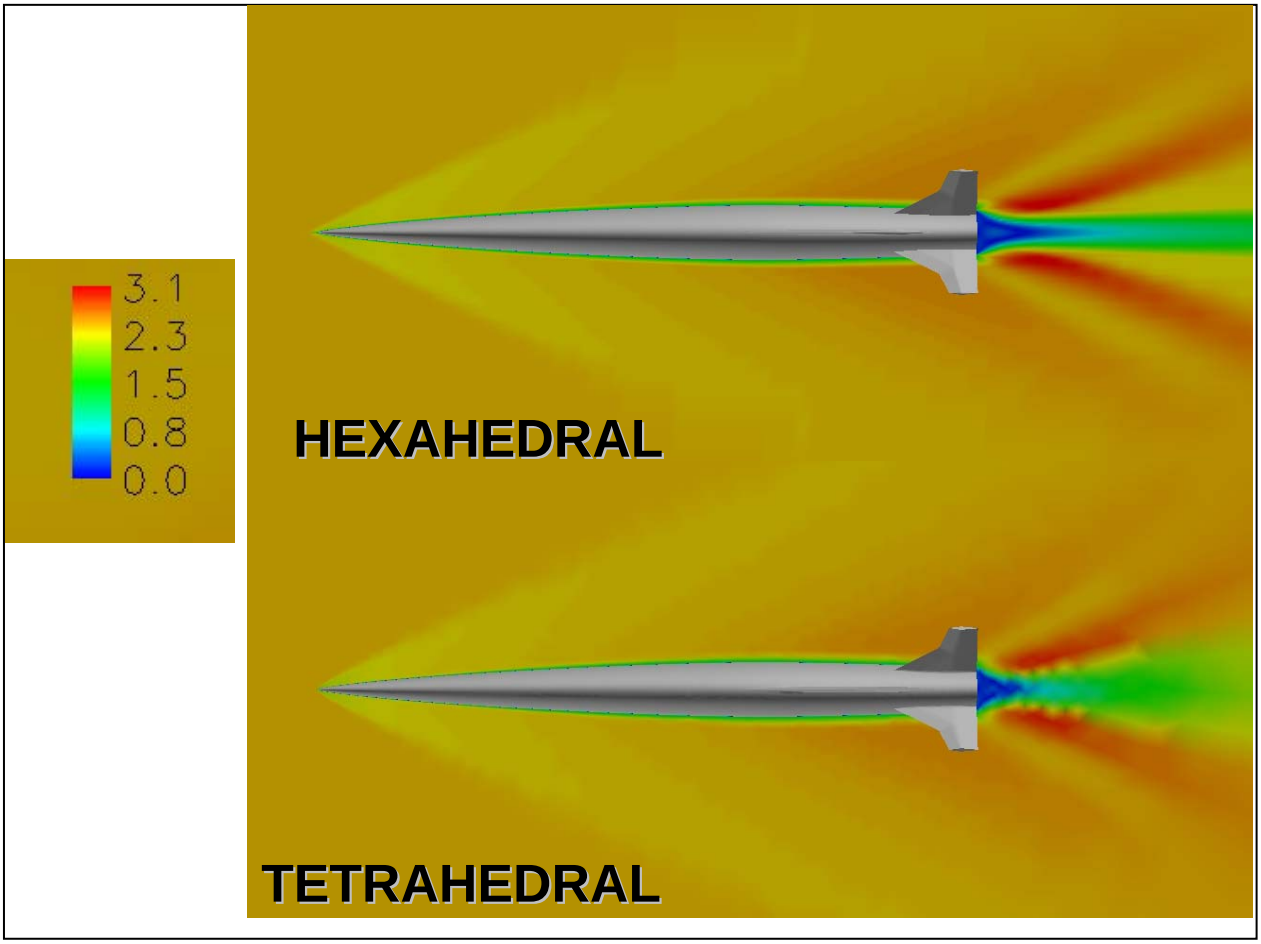

Figure 7. Mach contours for $\alpha = 0°$, $\phi = 0°$.

particularly noticeable in the flow behind the missile. In this region, the contours for the tetrahedral mesh are somewhat diffused, but may be artifacts of the contouring routine. Figure 8 depicts a similar finding in the circumferential plane in the area of the tail fins. The details of the pressure contours are more highly defined for the hexahedral case, especially on the lower tail fins, while the contours for the tetrahedral case are less distinct.

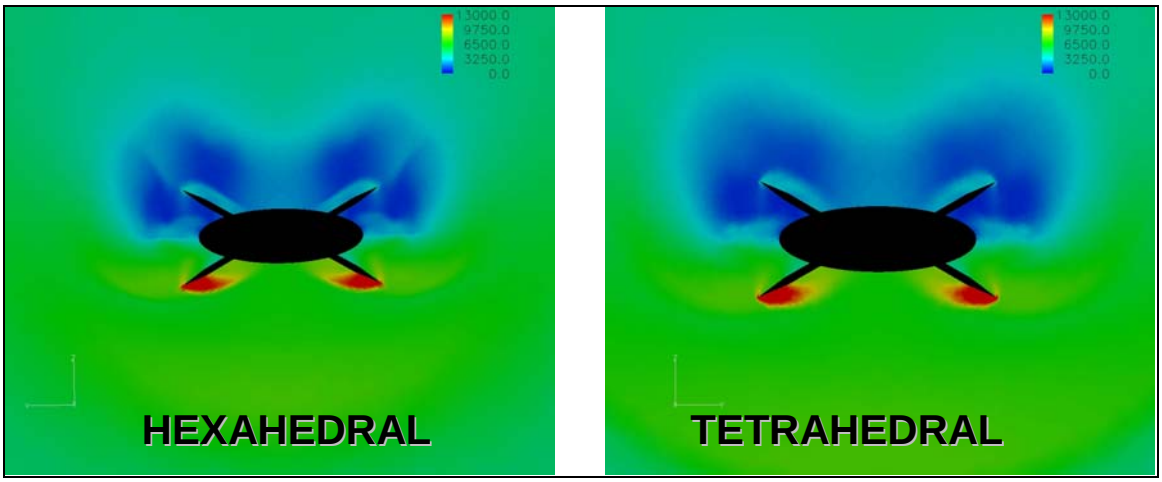

Figure 8. Pressure contours at x/L = 0.95, α = 15°, and ϕ = 0°.

The next series of figures show circumferential pressure contours at various axial locations for some of the different cases computed. The color map used depicts the pressure range in Pascals, from 0 (blue) to 13,500 (red). Since the flow fields for both grids show very similar features, only the results using the hexahedral grid are presented.

Figures 9–11 show the circumferential pressure contours for the missile with 0° roll angle at angles of attack of 5°, 15°, and 20°. The axial locations selected represent the flow around the missile on the ogive (x/L = 0.3 and 0.6), on the wings (x/L = 0.7 and 0.85), and on the tail fins (x/L = 0.95). As the angle of attack increased, the pressure on the lower surface of the body, wings, and bottom set of fins increases. The flow is symmetric on either side of the y = 0 plane.

Figure 12 shows the change in flow field when a yaw angle of 8.6° is added to the computational parameters for the 20° angle of attack case. The flow field becomes asymmetric and pressure increases on the left side of the missile.

Similar cases were computed with the missile at a roll angle of 45°. Figures 13–16 show circumferential pressure contours for the same four case studies. As the visual locations move down the missile, the changes in the flow field on the ogive, wings, and tail fins can be seen. As the angle of attack increases, the pressure on the lower surfaces of the body, fins, and wings increases also. At α = 15°, there is higher pressure on the inner surfaces of the bottom fins and the pressure involves both inner and outer surfaces at α = 20°. The addition of the yaw angle to the 20° case appears to cause the pressure to become more localized on the tip of the bottom fins.

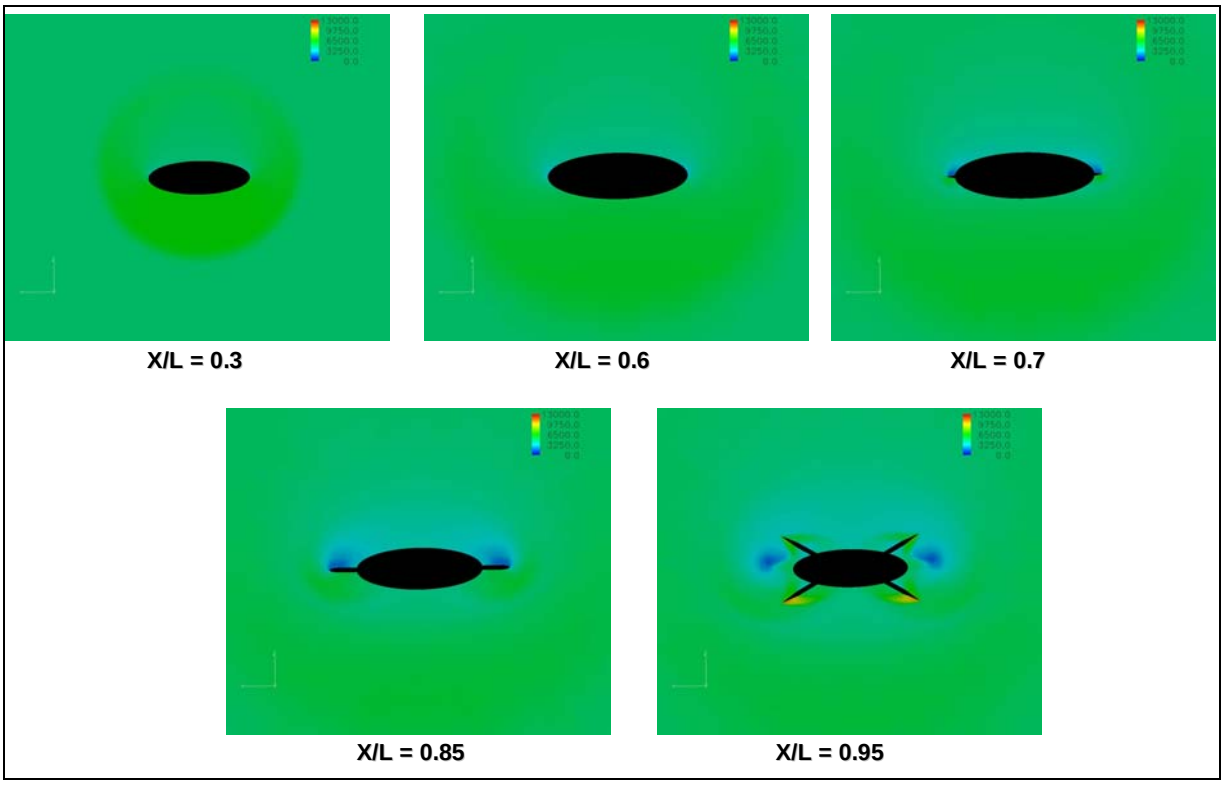

Figure 9. Circumferential pressure contours for $\phi = 0°$, $\alpha = 5°$.

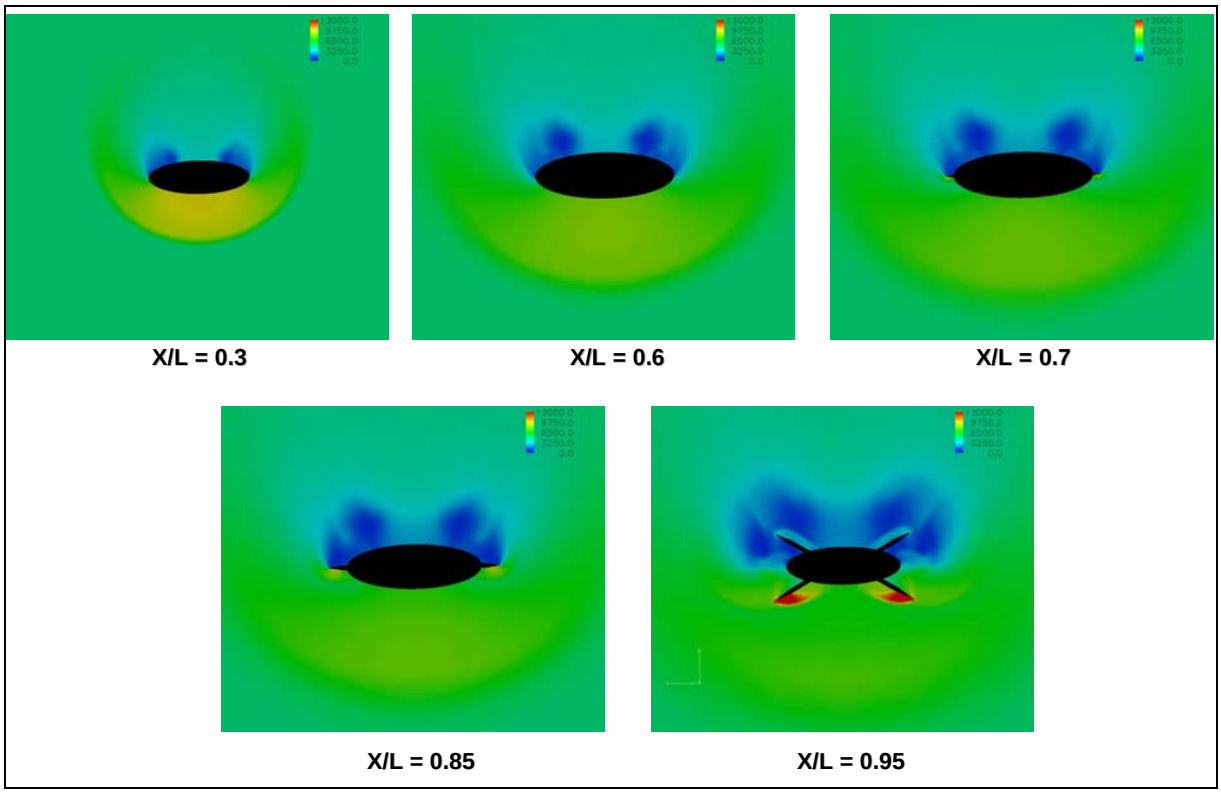

Figure 10. Circumferential pressure contours for $\phi = 0°$, $\alpha = 15°$.

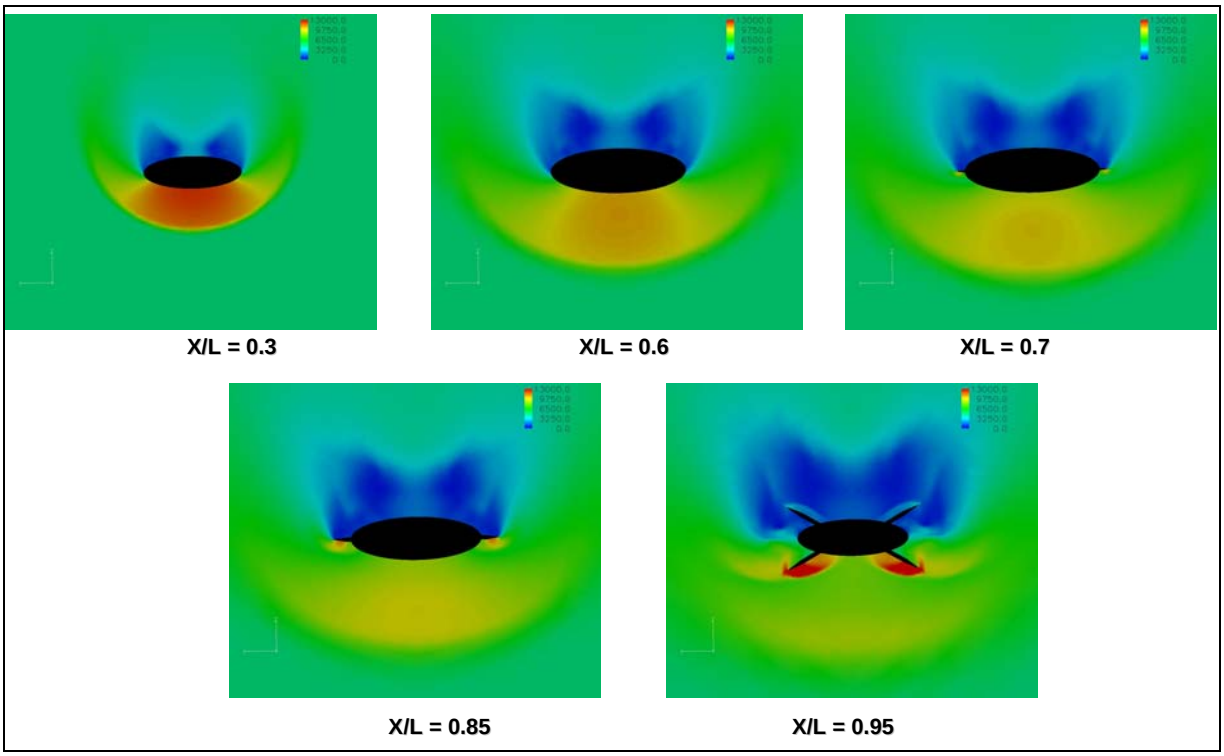

Figure 11. Circumferential pressure contours for $\phi = 0°$, $\alpha = 20°$.

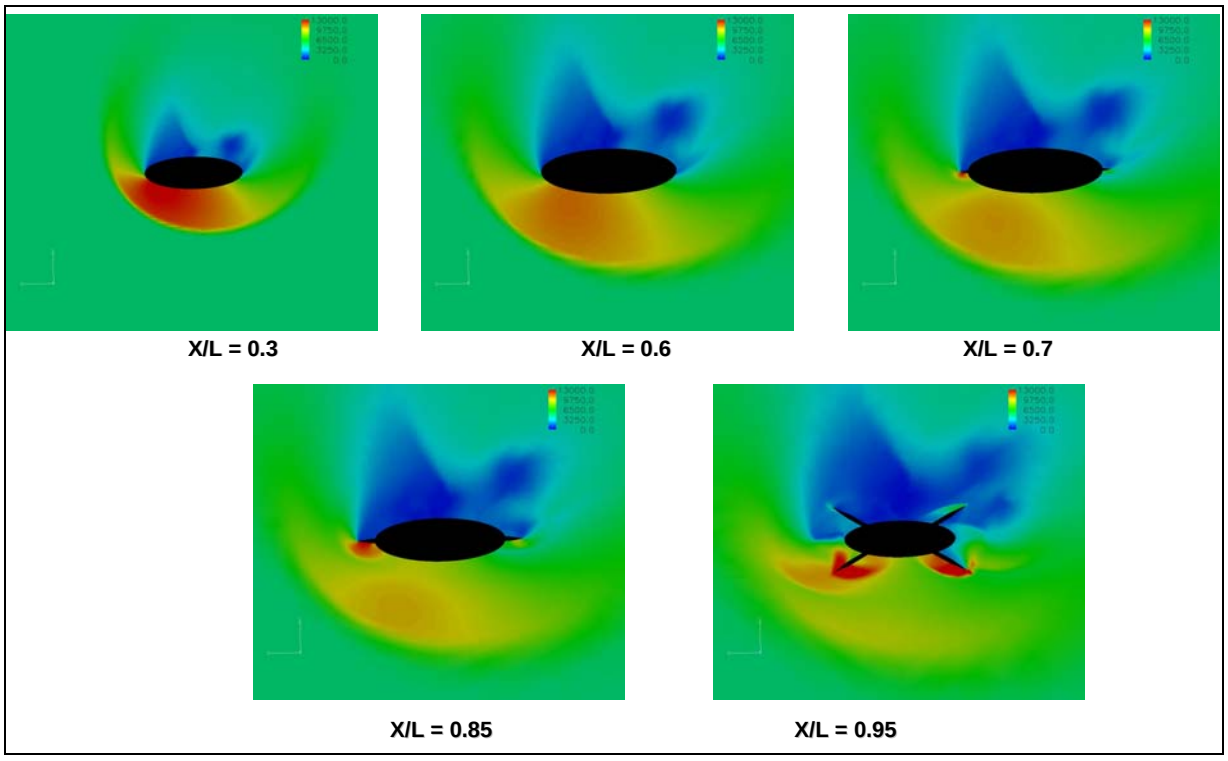

Figure 12. Circumferential pressure contours for $\phi = 0°$, $\alpha = 20°$, and $\beta = 8.6°$.

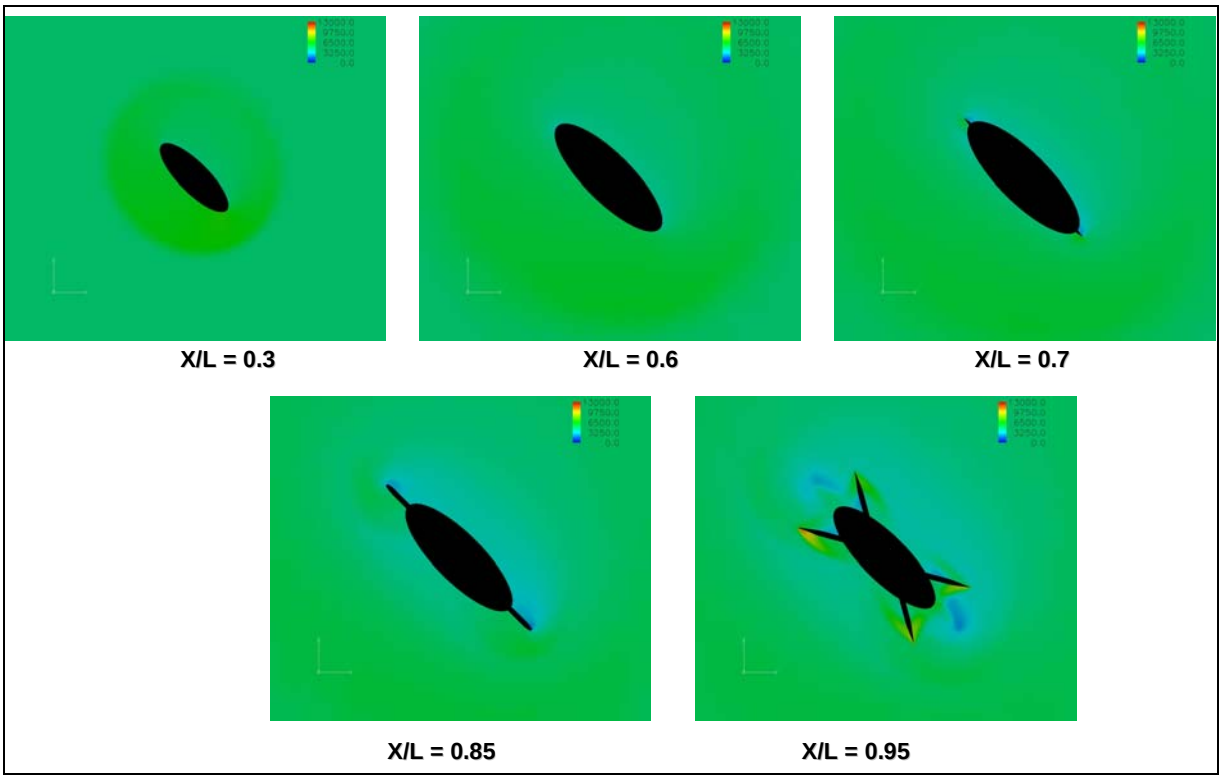

Figure 13. Circumferential pressure contours for $\phi = 45°$, $\alpha = 5°$.

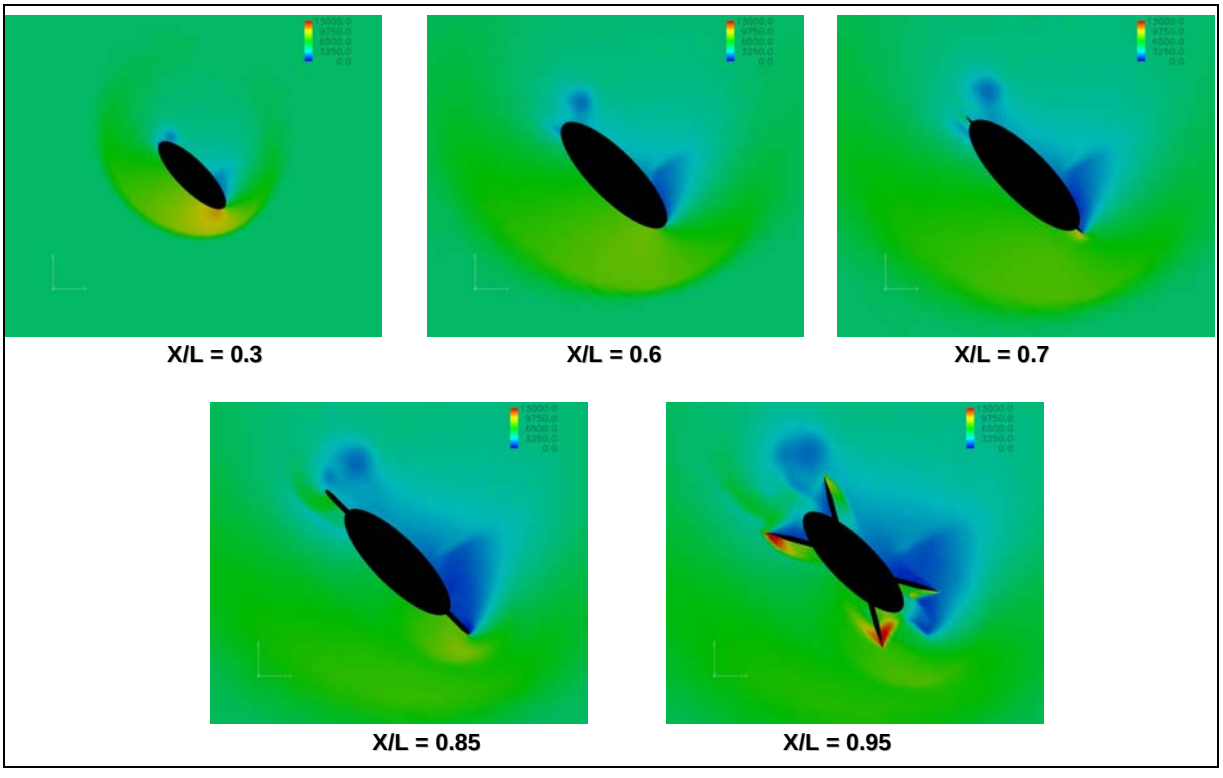

Figure 14. Circumferential pressure contours for $\phi = 45°$, $\alpha = 15°$.

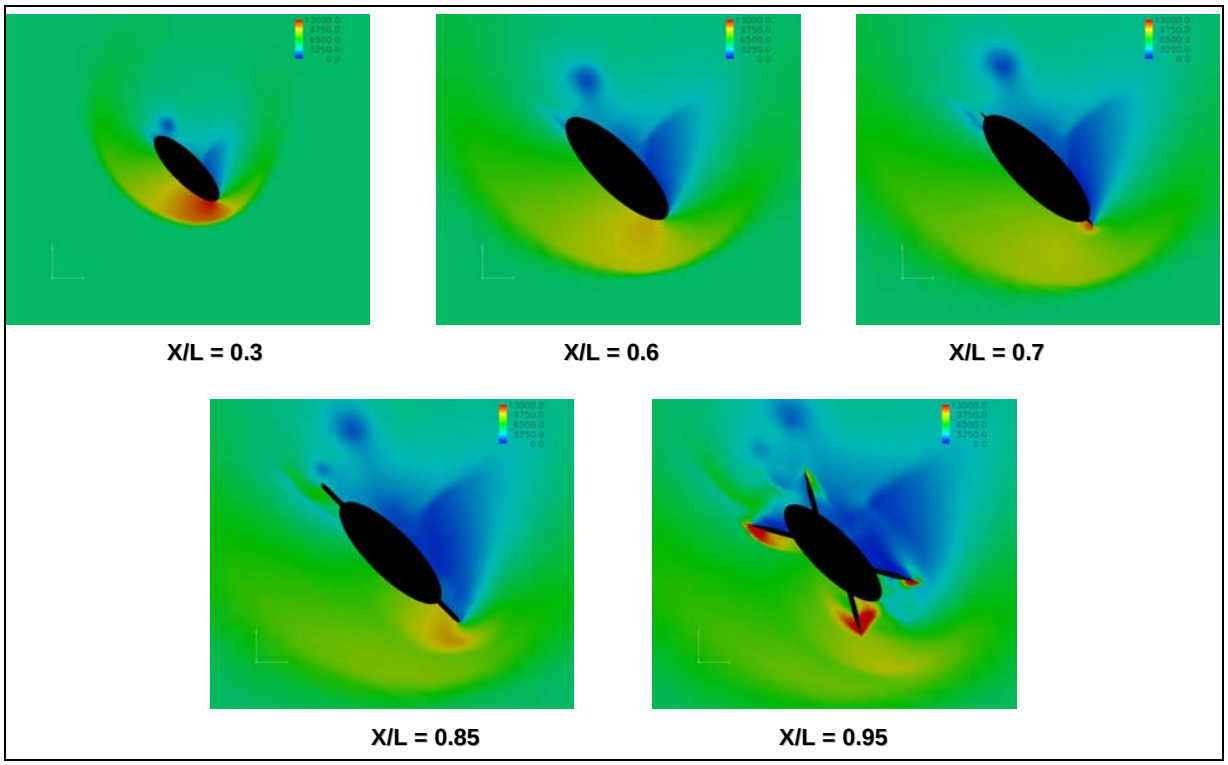

Figure 15. Circumferential pressure contours for $\phi = 45°$, $\alpha = 20°$.

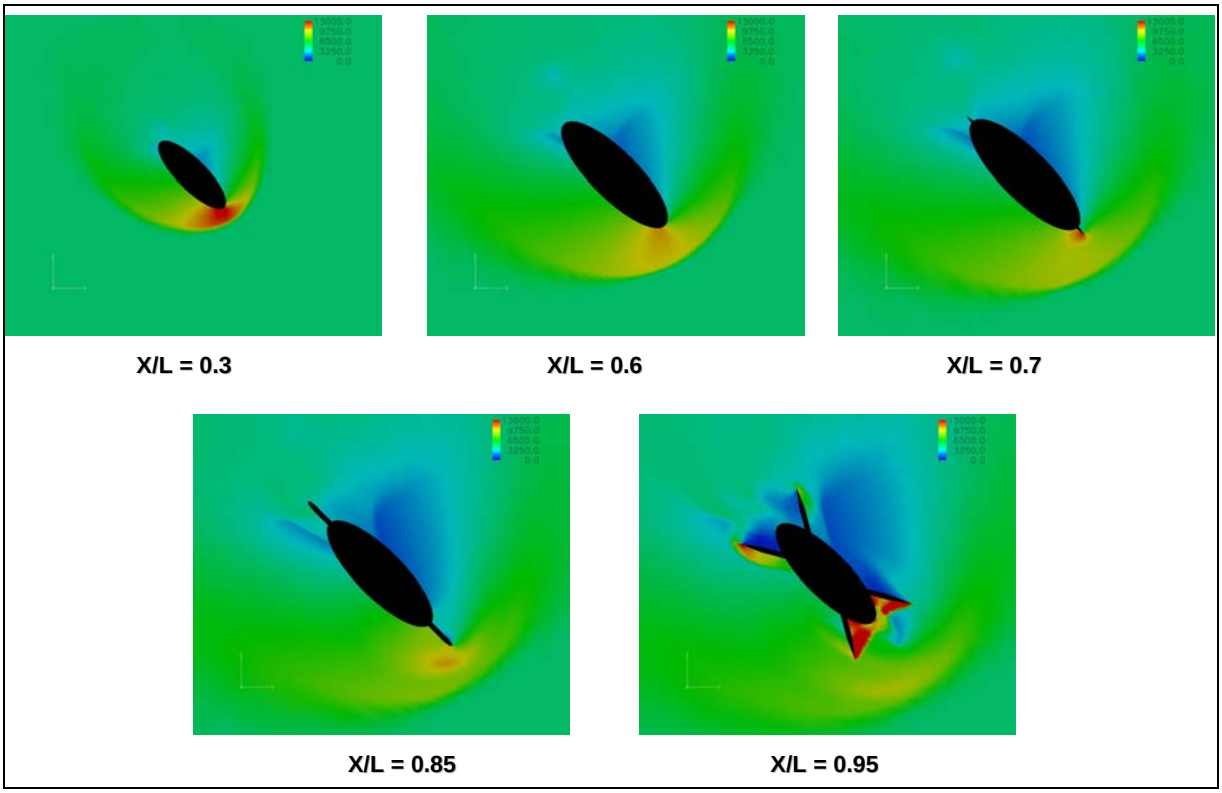

Figure 16. Circumferential pressure contours for $\phi = 45°$, $\alpha = 20°$, and $\beta = 8.6°$.

4.2 Quantitative Results

Circumferential pressure data extracted from the numerical solutions at axial locations of x/L = 0.3, 0.6, and 0.95 show the computed data from both grids to be similar and in good agreement with the experimental data. Figures 17–19 depict the comparisons for the 0° roll orientation. In general, there is good agreement in all the locations examined. For x/L = 0.3 and α = 15° and 20°, there is a slight difference in the numerical solutions in the θ = 30°–60° range, and again in the 300°–360° range. There is a noticeable discrepancy at x/L = 0.3, where the computed data does not match the experimental data at θ = 45° for the three angles of attack examined. As this experimental data point appears to be an outlier (i.e., it does not lie in line with the other data), it is possible that the experimental data is suspect here rather that the CFD calculation.

Similar plots are presented for the 45° roll missile configuration. Figures 20–22 show good agreement for all axial locations examined. There is little noticeable difference between numerical solutions for the hexahedral and tetrahedral grids. With the exception of the data point at θ = 45° for x/L = 0.3, there is good agreement between the numerical and experimental data.

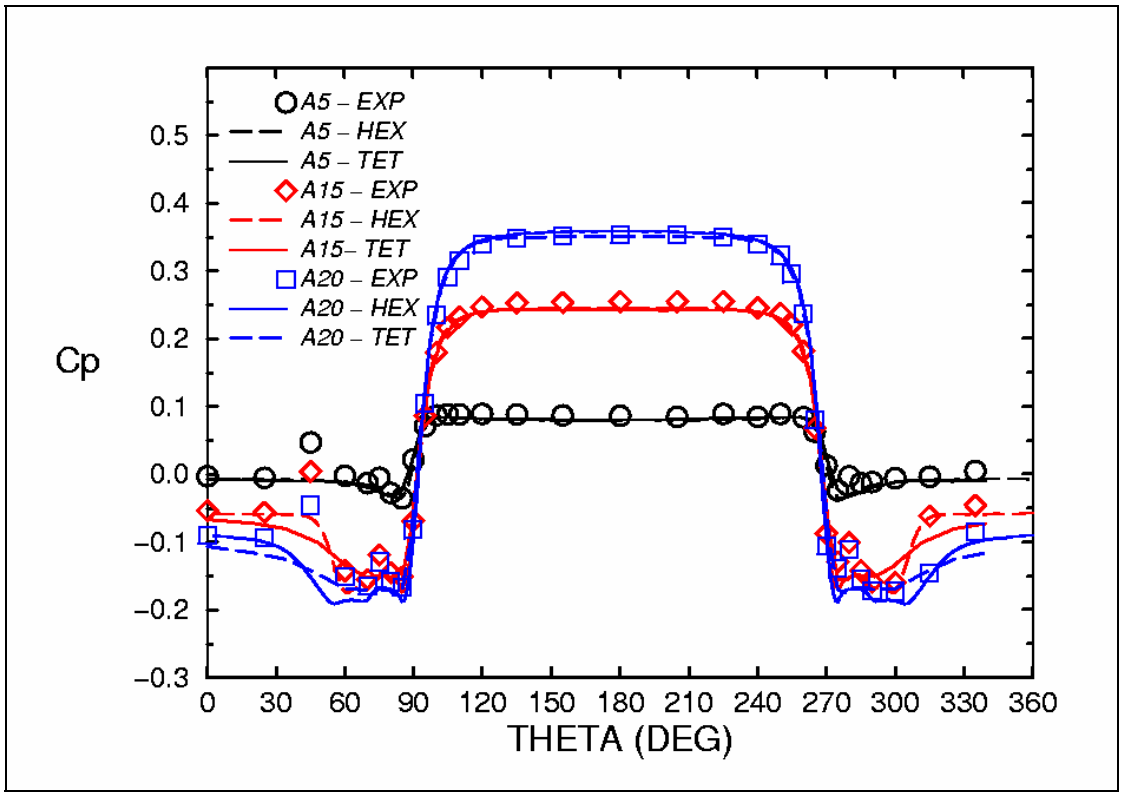

Figure 17. Circumferential pressure at x/L = 0.3, ϕ = 0°.

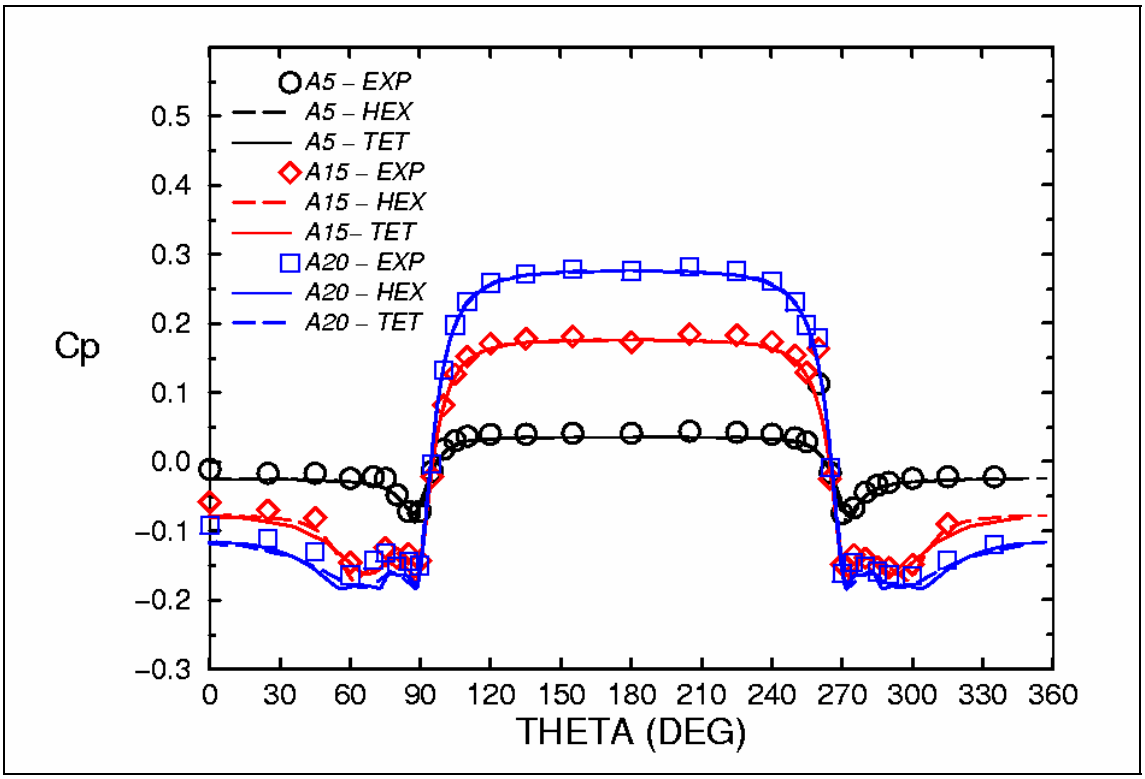

Figure 18. Circumferential pressure at x/L = 0.6, ϕ = 0°.

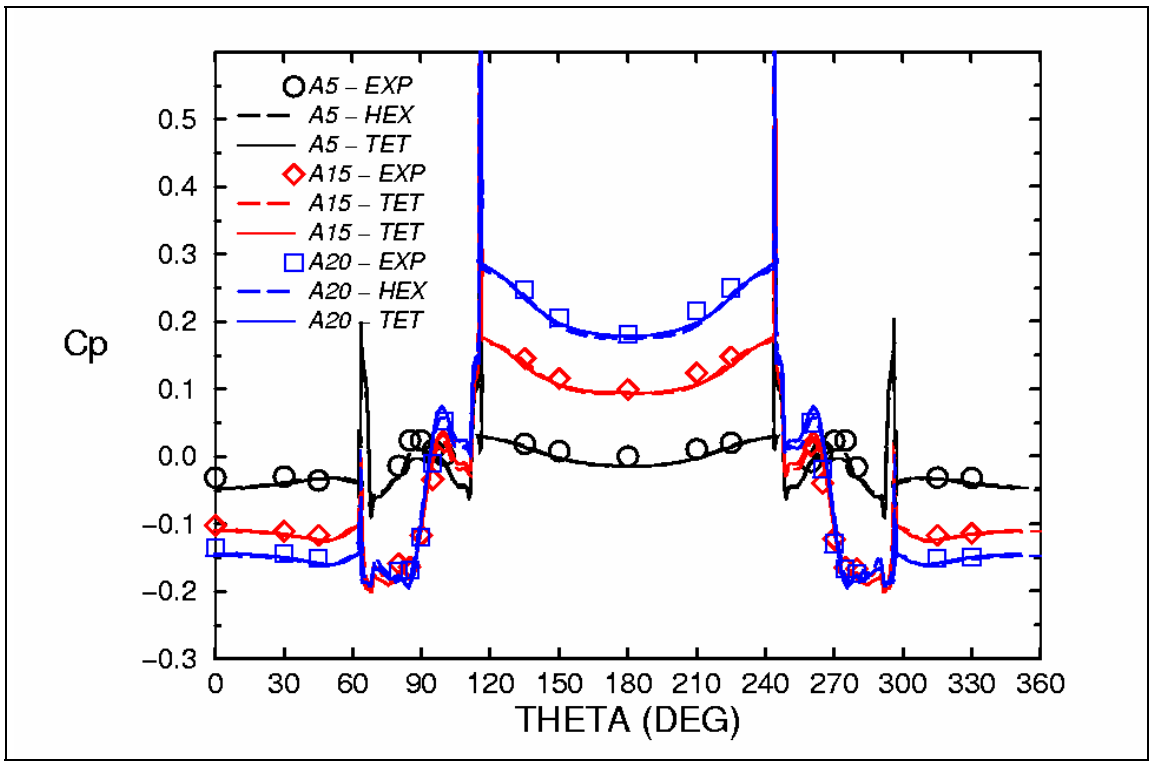

Figure 19. Circumferential pressure at x/L = 0.95, ϕ = 0°.

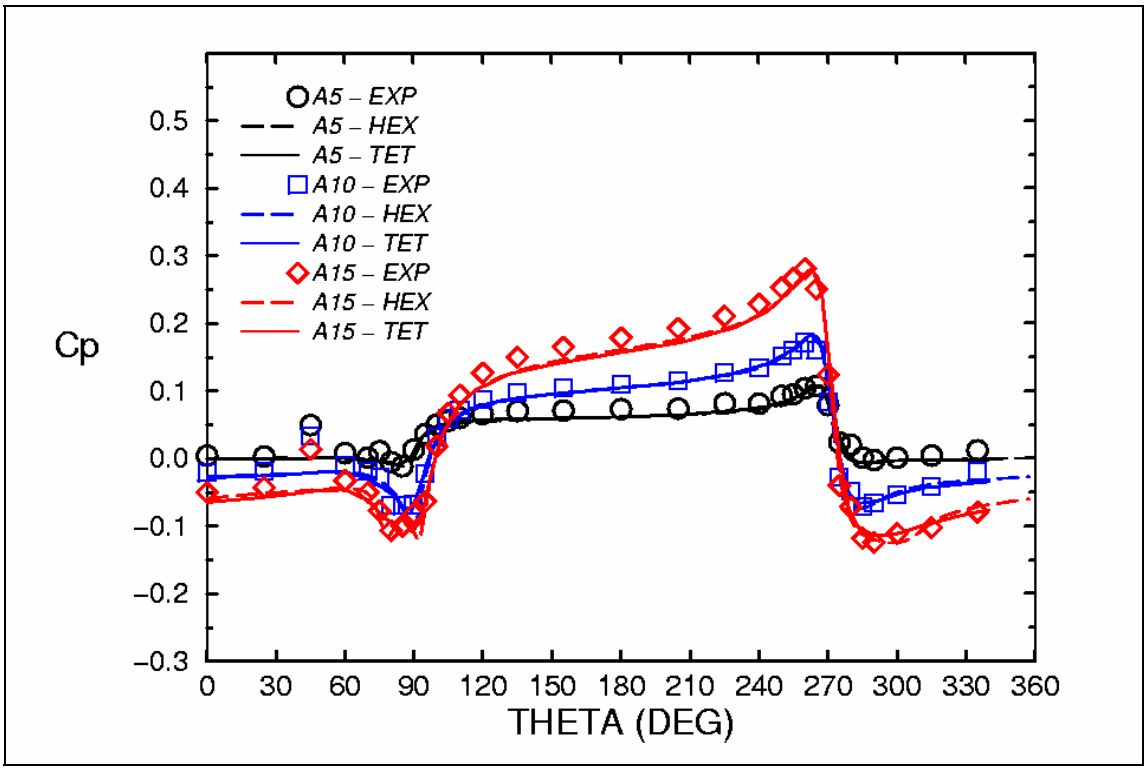

Figure 20. Circumferential pressure plots for x/L = 0.3, ϕ = 45°.

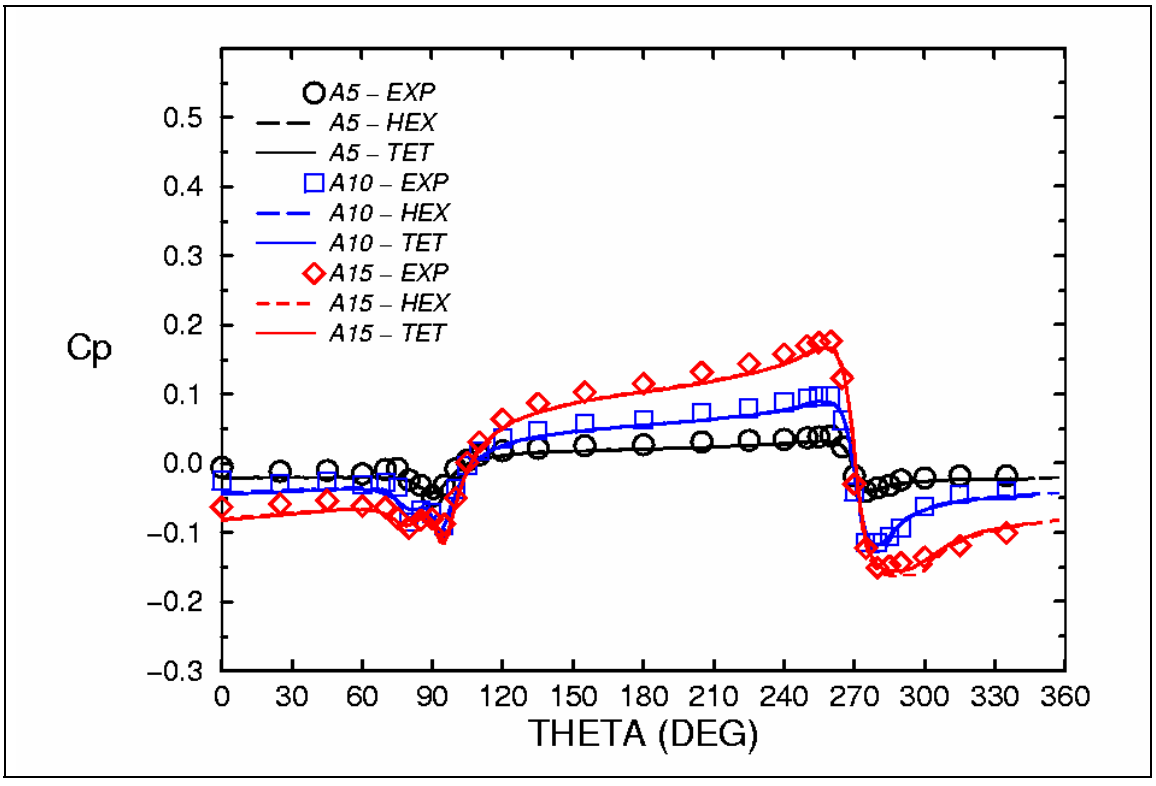

Figure 21. Circumferential pressure at x/L = 0.6, ϕ = 45°.

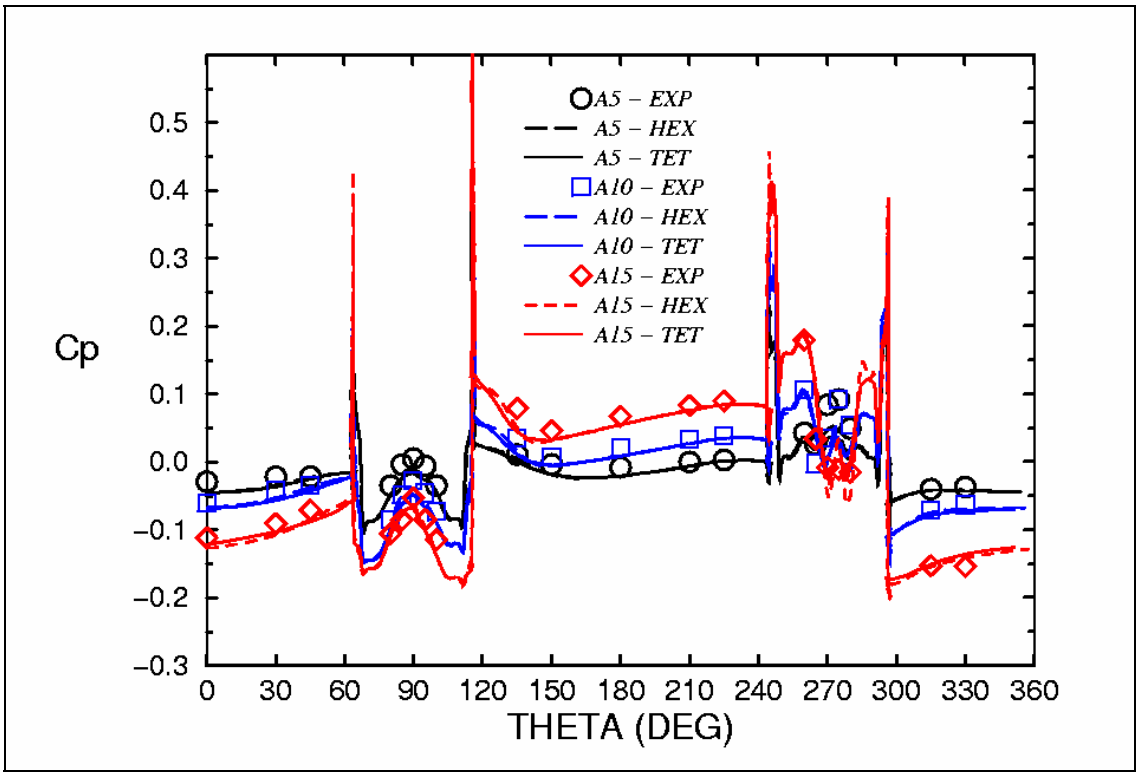

Figure 22. Circumferential pressure at x/L = 0.95, ϕ = 45°.

4.3 Comparison of Force and Moment Data

Force and moment data are compared with the available experimental data in the following tables. The computed axial forces (C_N) for both grid solutions are similar and compare quite well with the available experimental data. The data presented in table 1 shows excellent comparison of C_N for the 0° roll orientation cases. Tables 2 and 3 show data comparisons for cases with yaw angles of 4.6° and 8.6°, respectively. The experimental data for these cases was approximated visually from graphical representations found in Graves (*23*). Due to a difference in coordinate system orientation (for the *x*-axis), the experimental values for C_l (rolling moment) and C_n (side moment) were adjusted by changing the sign (*). The side force (C_Y) was not changed. With this modification, there is reasonable agreement between the two computations and the experimental data.

Table 1. Normal force (C_N) for 0° roll orientation.

Angle of Attack	Structured Grid	Unstructured Grid	Experiment
5	1.132	1.148	1.2
10	2.468	2.486	2.4
15	3.978	3.984	4.0
20	5.529	5.553	5.6

Table 2. Force and moments, $\phi = 0°$, $\alpha = 20°$, $\beta = 4.6°$.

	Structured Grid	**Unstructured Grid**	**Experiment* (approx)**
C_l	0.300	0.288	0.28
C_n	–0.219	–0.216	–0.23
C_Y	–0.292	–0.317	–0.27

Table 3. Force and moments, $\phi = 0°$, $\alpha = 20°$, $\beta = 8.6°$.

	Structured Grid	**Unstructured Grid**	**Experiment* (approx)**
C_l	0.495	0.495	0.48
C_n	–0.357	–0.342	–0.35
C_Y	–0.537	–0.575	–0.50

There was no experimental data available for similar cases for the missile at a 45° roll orientation, but the computed values for C_N shown in table 4 show excellent agreement between the two computational solutions. With the exception of C_l (table 5) and C_n (table 6), the computational data for yaw angles 4.6° and 8.6° show reasonable similarity for this missile orientation also.

Table 4. Normal force (C_N) for 45° roll orientation.

Angle of Attack	**Structured Grid**	**Unstructured Grid**
5	0.684	0.696
10	1.472	1.491
15	2.422	2.437
20	3.372	3.341

Table 5. Force and moments, $\phi = 45°$, $\alpha = 20°$, $\beta = 4.6°$.

	Structured Grid	**Unstructured Grid**
C_l	0.669	0.612
C_n	–0.327	0.343
C_y	1.414	1.426

Table 6. Force and moments, $\phi = 45°$, $\alpha = 20°$, $\beta = 8.6°$.

	Structured Grid	Unstructured Grid
C_l	0.533	0.529
C_n	–0.431	0.494
C_y	0.716	0.714

The computational data used in tables 1–6, along with additional computational data not examined as part of this study, is presented in the appendix.

5. Summary and Conclusions

Numerical computations using viscous Navier-Stokes methods were performed to predict the flow field and aerodynamic coefficients on a geometrically complex missile configuration under wind tunnel test conditions. Full 3-D computations were performed and no symmetry was used. Computational results were obtained for a complex NASA missile configuration with elliptic cross section and multiple fins, at supersonic speed for various roll orientations and angles of attack, using a two-equation k-ε turbulence model. Numerical results show the qualitative features (vortices and cross-flow separation regions) of flow field at various axial and streamwise positions along the model configurations. Aerodynamic coefficients have been obtained from the computed solutions and found to match well with the available experimental data for this configuration. These numerical results show that modern CFD techniques such as the one used in the present computational study are capable of accurately predicting the aerodynamics of complex missile configurations.

6. References

1. Sahu, J.; Heavey, K. R.; Ferry, E. N. Computational Fluid Dynamics for Multiple Projectile Configurations. *Proceedings of the 3rd Overset Composite Grid and Solution Technology Symposium*, Los Alamos, NM, October 1996.

2. Sahu, J.; Heavey, K. R.; Nietubicz, C. J. Time-Dependent Navier-Stokes Computations for Submunitions in Relative Motion. *6th International Symposium on Computational Fluid Dynamics*, Lake Tahoe, NV, September 1995.

3. Meakin, R. L. Computations of the Unsteady Flow About a Generic Wing/Pylon/Finned-Store Configuration; AIAA 92-4568-CP, August 1992.

4. Sahu, J.; Heavey, K. R.; Edge, H. L. *Numerical Computations of Supersonic Flow Over Elliptic Projectiles*; ARL-TR-2589; U.S. Army Research Laboratory: Aberdeen Proving Ground, MD, December 2001.

5. Sahu, J.; DeSpirito, J.; Edge, H.; Silton, S.; Heavey, K. Recent Applications of Structured and Unstructured Grid Techniques to Complex Projectile and Missile Configurations. *Proceedings of the Eighth International Grid Generation and Computational Field Simulations*, Honolulu, HI, June 2002.

6. Pagan, D.; Molton, P.; Delery, J. Basic Experiment on a Supersonic Vortex Flow Around a Missile Body. *Journal of Spacecraft and Rockets* **1992**, *29* (3), 373–378.

7. Grasso, F.; Iaccarino, G. Influence of Crossflow and Turbulence on Vortex Flow Around a Supersonic Missile. *Journal of Spacecraft and Rockets* **1998**, *35* (1), 37–45.

8. Sahu, J.; Heavey, K. R. Application of CFD to High Angle of Attack Missile Flowfields, *18th Applied Aerodynamics Meeting*; AIAA Paper No. 2000-4210, Denver, CO, August 2000.

9. Birch, T.; Wrisdale, I. E.; Prince, S. CFD Predictions of Missile Flowfields, *18th Applied Aerodynamics Meeting*; AIAA Paper No. 2000-4211, Denver, CO, August 2000.

10. Birch, T.; Allen, J.; Wilcox, F. J. Force, Surface Pressure and Flowfield Measurements on Slender Missiles at Supersonic Speeds, *18th Applied Aerodynamics Meeting*; AIAA Paper No. 2000-4207, Denver, CO, August 2000.

11. Edwards, J. A.; Roper, J. J. A Computational Assessment of Static and Dynamic Coefficients for the H3 Hypervelocity Projectile, AIAA Paper 97-0640, January 1997.

12. Orchard, D.; Fournier, E.; Dupuis, A.; Edwards, J. Wind Tunnel Tests on the H3P78, Power Law, Elliptic Section Flared Projectile From Mach 2.5 to 4, AIAA Paper No. 2001-4321, Montreal, Canada, August 2001.

13. Fournier, E.; Orchard, D. *Testing of a Novel Maneuvering Projectile in the DREV Trisonic Wind Tunnel*; Technical Memorandum Report, DREV TM-2000-108, Canada, July 2000.

14. Sahu, J.; Heavey, K. R.; Edge, H. L. Numerical Computations of Supersonic and Hypersonic Flow Over Elliptical Projectiles, *Atmospheric Flight Mechanics Conference*; AIAA Paper No. 2001-4320, Montreal, Canada, August 2001.

15. Orchard, D.; Fournier, E.; Dupuis, A.; Edwards, J. Wind Tunnel Tests on the H3P78, Power Law, Elliptic Section Flared Projectile With Jet Interaction, AIAA Paper No. 2001-4322, Montreal, Canada, August 2001.

16. Sahu, J. Numerical Simulations of Supersonic Flow Over an Elliptic-Section Projectile With Jet Interaction, *AIAA Applied Aerodynamics Conference*; AIAA Paper No. 2002-3260, St. Louis, MO, June 2002.

17. Sahu, J.; Silton, S. I.; Heavey, K. R. Numerical Computations of Supersonic Flow Over Nonaxisymmetric Configurations, *Applied Aerodynmacis Conference*; AIAA Paper No. 2004-5456, Providence, RI, 2004.

18. Allen, J. M.; Hernandez, G.; Lamb, M. *Body-Surface Pressure Data on Two Monoplane-Wing Missile Configurations With Elliptical Cross-Sections at Mach 2.50*; NASA Technical Memorandum 85645; NASA Langley Research Center: Hampton, VA, 1983.

19. Peroomian, O.; Chakravarthy, S.; Goldberg, U. A Grid-Transparent Methodology for CFD; AIAA Paper 97-07245, 1997.

20. Peroomian, O.; Chakravarthy, S.; Palaniswamy S.; Goldberg, U. Convergence Acceleration for Unified-Grid Formulation Using Preconditioned Implicit Relaxation; AIAA Paper 98-0116, 1998.

21. Pulliam, T. H.; Steger, J. L. On Implicit Finite-Difference Simulations of Three-Dimensional Flow. *AIAA Journal* **1982**, *18* (2), 159–167.

22. Goldberg, U. C.; Peroomian, O.; Chakravarthy, S. A Wall-Distance-Free k-ε Model With Enhanced Near-Wall Treatment. *ASME Journal of Fluids Engineering* **1998**, *120*, 457–462.

23. Graves, E. B. *Aerodynamic Characteristics of a Monoplanar Missile Concept With Bodies of Circular and Elliptical Cross-Sections*; NASA Technical Memorandum 74079; NASA Langley Research Center: Hampton, VA, 1977.

24. Graves, E. B.; Fournier, R. H. *Effect of Nose Bluntness and Afterbody Shape on Aerodynamic Characteristics of a Monoplanar Missile Concept With Bodies of Circular and Elliptical Cross-Sections at a Mach Number of 2.50*; NASA Technical Memorandum 80055; NASA Langley Research Center: Hampton, VA, 1979.

25. Allen, J. NASA Langley Research Center: Hampton, VA. Private communications, 2003.

26. Burnley, V.; Hoke, C.; Schwabacher, G. Aerodynamic Analysis of Complex Missile Configurations Using AVUS (Air Vehicles Unstructured Flow Solver), *Applied Aerodynamics Meeting*; AIAA Paper No. 2004-5452, Providence, RI, 2004.

Appendix. Computational Data

A.1 Missile With Elliptic Cross Section, Mach = 2.5, Yaw Angle = 0°

	Orientation	Grid Type
Case I	0° roll	Tetrahedral
Case II	45° roll	Tetrahedral
Case III	0° roll	Hexahedral
Case IV	45° roll	Hexahedral

Pressure	4761.81 Pa
Density	0.1098 kg/s
Velocity	616.0
Spin, p	8944
Reference diameter	10.16 cg
Reference area	0.008107 m^2
Speed, sound	2.45.4 m/s
Center of gravity	4.2 cal
qS	168.89

qS=dynamic press* reference area

		Aerodynamic Coefficients					
Case	**Alpha**	**C_X**	**C_Y**	**C_N**	**C_m**	**C_n**	**C_l**
I	0	0.30946	0.00010	0.00047	0.00056	0.00020	–0.00015
I	5	0.30339	0.00002	1.14776	–0.09334	–0.00005	–0.00003
I	10	0.30496	0.00004	2.48607	–0.08904	–0.00068	–0.00029
I	15	0.32164	–0.00009	3.98372	–0.06929	–0.00007	0.00014
I	20	0.34078	0.00002	5.53302	–23.41887	0.00012	0.00001
II	0	0.30940	0.00052	0.00050	0.00006	–0.00012	–0.00010
II	5	0.30740	0.43594	0.69628	–0.16889	–0.07070	0.07114
II	10	0.30763	0.92257	1.49089	–0.31743	–0.15739	0.26721
II	15	0.30703	1.50634	2.43654	–0.49145	–0.26965	0.52974
II	20	0.35109	2.22719	3.34118	–0.50319	–0.29161	0.65374
III	0	0.29565	–0.00012	–0.00002	0.00007	–0.31208	–0.00009
III	5	0.29018	–0.00003	1.13152	–0.09817	–0.00004	0.00003
III	10	0.29009	0.00008	2.46824	–0.07974	0.00013	0.00008
III	15	0.30479	–0.00028	3.97936	–0.07300	0.00006	–0.01035
III	20	0.32900	0.00007	5.52991	0.10791	0.00006	0.00003
IV	0	0.29673	–0.00001	0.00000	0.00000	–0.00001	–0.00004
IV	5	0.29504	0.43123	0.68381	–0.16375	–0.06396	0.07318
IV	10	0.29504	0.91835	1.47230	–0.30868	–0.13460	0.27076
IV	15	0.30064	1.51329	2.42211	0.38195	–0.81232	0.54848
IV	20	0.32266	2.18825	3.37210	–0.52519	–0.28050	0.65656

CFD++ Forces and Moments

Case	Alpha	FX	FY	FZ	MX	MY	MZ
I	0	5.23E + 01	1.61E - 02	7.87E - 02	–2.55E - 03	9.56E - 03	3.39E - 03
I	5	5.12E + 01	3.30E - 03	1.94E + 02	–4.99E - 04	–1.60E + 00	–8.91E - 04
I	10	5.15E + 01	6.42E - 03	4.20E + 02	–4.89E - 03	–1.53E + 00	–1.17E - 02
I	15	5.43E + 01	–1.53E - 02	6.73E + 02	2.34E - 03	–1.19E + 00	–1.15E - 03
I	20	5.76E + 01	2.76E - 03	9.34E + 02	1.96E - 04	–4.02E + 02	2.10E - 03
II	0	5.23E + 01	8.72E - 02	8.48E - 02	–1.66E - 03	1.10E - 03	–2.02E - 03
II	5	5.19E + 01	7.36E + 01	1.18E + 02	1.22E + 00	–2.90E + 00	–1.21E + 00
II	10	5.20E + 01	1.56E + 02	2.52E + 02	4.59E + 00	–5.45E + 00	–2.70E + 00
II	15	5.19E + 01	2.54E + 02	4.12E + 02	9.09E + 00	–8.43E + 00	–4.63E + 00
II	20	5.93E + 01	3.76E + 02	5.64E + 02	1.12E + 01	–8.63E + 00	–5.00E + 00
III	0	4.99E + 01	–2.01E - 02	–4.06E - 03	–1.59E - 03	1.12E - 03	–5.36E + 00
III	5	4.90E + 01	–5.32E - 03	1.91E + 02	5.21E - 04	–1.68E + 00	–6.73E - 04
III	10	4.90E + 01	1.29E - 02	4.17E + 02	1.40E - 03	–1.37E + 00	2.19E - 03
III	15	5.15E + 01	–4.80E - 02	6.72E + 02	–1.78E - 01	–1.25E + 00	1.11E - 03
III	20	5.56E + 01	1.17E - 02	9.34E + 02	5.31E - 04	1.85E + 00	1.11E - 03
IV	0	5.01E + 01	–9.34E - 04	–4.44E - 04	–6.67E - 04	4.80E - 05	–1.75E - 04
IV	5	4.98E + 01	7.28E + 01	1.15E + 02	1.26E + 00	–2.81E + 00	–1.10E + 00
IV	10	4.98E + 01	1.55E + 02	2.49E + 02	4.65E + 00	–5.30E + 00	–2.31E + 00
IV	15	5.08E + 01	2.56E + 02	4.09E + 02	9.41E + 00	6.55E + 00	–1.39E + 01
IV	20	5.45E + 01	3.70E + 02	5.70E + 02	1.13E + 01	–9.01E + 00	–4.81E + 00

A.2 Missile With Elliptic Cross Section, Mach = 2.5, Yaw Angle = 4.6°

	Orientation	Grid Type
Case I	0° roll	Tetrahedral
Case II	45° roll	Tetrahedral
Case III	0° roll	Hexahedral
Case IV	45° roll	Hexahedral

Pressure	4761.81 Pa
Density	0.1098 kg/s
Velocity	616.0
Spin,p	8944
Reference diameter	10.16 cg
Reference area	0.008107 m^2
Speed, sound	2.45.4 m/s
Center of gravity	4.2 cal
qS	168.89

qS=dynamic press* reference area

Aerodynamic Coefficients

Case	Alpha	C_X	C_Y	C_N	C_m	C_n	C_l
I	20	0.33458	–0.31657	5.46295	–0.18056	–0.21573	0.28930
II	20	0.35480	1.42679	3.14192	–0.80731	–0.34279	0.61229
III	20	0.32130	–0.29218	5.47801	–0.04582	–0.21996	0.30001
IV	20	0.32275	1.41406	2.96861	–8.24658	–0.32749	0.66923

CFD++ Forces and Moments

Case	Alpha	FX	FY	FZ	MX	MY	MZ
I	20	5.65E + 01	–5.35E + 01	9.23E + 02	4.96E + 00	–3.10E + 00	–3.70E + 00
II	20	5.99E + 01	2.41E + 02	5.31E + 02	1.05E + 01	–1.39E + 01	–5.88E + 00
III	20	5.43E + 01	–4.93E + 01	9.25E + 02	5.15E + 00	–7.86E - 01	–3.77E + 00
IV	20	5.45E + 01	2.39E + 02	5.01E + 02	1.15E + 01	–1.42E + 02	–5.62E + 00

A.3 Missile With Elliptic Cross Section, Mach = 2.5, Yaw Angle = 8.6°

	Orientation	Grid Type
Case I	0 deg roll	Tetrahedral
Case II	45 deg roll	Tetrahedral
Case III	0 deg roll	Hexahedral
Case IV	45 deg roll	Hexahedral

Pressure	4761.81 Pa
Density	0.1098 kg/s
Velocity	616.0
Spin,p	8944
Reference Diameter	10.16 cg
Reference Area	0.008107 m^2
Speed, sound	2.45.4 m/s
Center of Gravity	4.2 cal
qS	168.89

qS=dynamic press* reference area

Aerodynamic Coefficients

Case	Alpha	C_X	C_Y	C_N	C_m	C_n	C_l
I	20	0.34159	–0.54755	5.60456	–0.15415	–0.34227	0.49468
II	20	0.34942	0.71394	2.59850	–0.84507	–0.49421	0.52901
III	20	0.33920	–0.53711	5.60275	–0.10027	–0.35737	0.49527
IV	20	0.32911	0.71618	2.55470	–0.85667	–0.43142	0.53300

CFD++ Forces and Moments

Case	Alpha	FX	FY	FZ	MX	MY	MZ
I	20	5.77E + 01	–9.25E + 01	9.47E + 02	8.49E + 00	–2.65E + 00	–5.87E + 00
II	20	5.90E + 01	1.21E + 02	4.39E + 02	9.08E + 00	–1.45E + 01	–8.48E + 00
III	20	5.73E + 01	–9.07E + 01	9.46E + 02	8.50E + 00	–1.72E + 00	–6.13E + 00
IV	20	5.56E + 01	1.21E + 02	4.31E + 02	9.15E + 00	–1.47E + 01	–7.40E + 00

NO. OF COPIES ORGANIZATION

1 (PDF ONLY) DEFENSE TECHNICAL INFORMATION CTR
DTIC OCA
8725 JOHN J KINGMAN RD
STE 0944
FORT BELVOIR VA 22060-6218

1 US ARMY RSRCH DEV & ENGRG CMD
SYSTEMS OF SYSTEMS INTEGRATION
AMSRD SS T
6000 6TH ST STE 100
FORT BELVOIR VA 22060-5608

1 INST FOR ADVNCD TCHNLGY
THE UNIV OF TEXAS
AT AUSTIN
3925 W BRAKER LN STE 400
AUSTIN TX 78759-5316

1 US MILITARY ACADEMY
MATH SCI CTR EXCELLENCE
MADN MATH
THAYER HALL
WEST POINT NY 10996-1786

1 DIRECTOR
US ARMY RESEARCH LAB
IMNE ALC IMS
2800 POWDER MILL RD
ADELPHI MD 20783-1197

3 DIRECTOR
US ARMY RESEARCH LAB
AMSRD ARL CI OK TL
2800 POWDER MILL RD
ADELPHI MD 20783-1197

3 DIRECTOR
US ARMY RESEARCH LAB
AMSRD ARL CS IS T
2800 POWDER MILL RD
ADELPHI MD 20783-1197

NO. OF COPIES ORGANIZATION

ABERDEEN PROVING GROUND

1 DIR USARL
AMSRD ARL CI OK TP (BLDG 4600)

NO. OF
COPIES ORGANIZATION

1 COMMANDER
NSWC
CODE B40
W YANTA
DAHLGREN VA 22448-5100

1 COMMANDER
NSWC
CODE 420
A WARDLAW
INDIAN HEAD MD 20640-5035

1 AIR FORCE ARMAMENT LAB
AFATL/FXA
D BELK
EGLIN AFB FL 32542-5434

3 COMMANDER
US ARMY TACOM ARDEC
AMSTA AR FSF T
BLDG 382
J GRAU
H HUDGINS
W KOENIG
PICATINNY ARSENAL NJ 07806-5000

1 COMMANDER
US ARMY TACOM
AMSTA AR CCH B
P VALENTI
BLDG 65-S
PICATINNY ARSENAL NJ 07806-5001

1 COMMANDER
US ARMY ARDEC
SFAE FAS SD
M DEVINE
PICATINNY ARSENAL NJ 07806-5001

1 NAWC
D FINDLAY
MS 3 BLDG 2187
PATUXENT RIVER MD 20670

1 UNIV OF ILLINOIS AT URBANA
CHAMPAIGN
DEPT OF MECHANICAL AND
INDUSTRIAL ENGINEERING
J C DUTTON
URBANA IL 61801

NO. OF
COPIES ORGANIZATION

1 COMMANDER
US ARMY TACOM ARDEC
BLDG 162S
AMCPM DS MO
P J BURKE
PICATINNY ARSENAL NJ 07806-5000

ABERDEEN PROVING GROUND

16 DIR USARL
AMSRD ARL CI HC
R NOAK
AMSRD ARL WM
J SMITH
AMSRD ARL WM B
T KOGLER
AMSRD ARL WM BA
D LYON
AMSRD ARL WM BC
J DESPIRITO
B GUIDOS
K HEAVEY (3 CPS)
J NEWILL
P PLOSTINS
J SAHU
S SILTON
P WEINACHT
AMSRD ARL WM BD
B FORCH
AMSRD ARL WM BF
S WILKERSON

NO. OF COPIES	ORGANIZATION
1	JOHN A EDWARDS DSTL FELLOW MCM DEPARTMENT DSTL FORT HALSTEAD SEVEN OAKS KENT NT14 7BP UK

INTENTIONALLY LEFT BLANK.